**Supporting Information**

# Construction of an Enzyme-free Concatenated DNA Circuit for Signal Amplification and Intracellular Imaging

*Huimin Wang,*[a] *Chunxiao Li,*[a] *Xiaoqing Liu,*[a] *Xiang Zhou,*[b] *Fuan Wang*[a]*

[a] Key Laboratory of Analytical Chemistry for Biology and Medicine (Ministry of Education), College of Chemistry and Molecular Sciences, Wuhan University, Wuhan 430072, P. R. China

[b] Key Laboratory of Biomedical Polymers-Ministry of Education, College of Chemistry and Molecular Sciences, Wuhan University, 430072 Wuhan, P. R. China.

[*] To whom correspondence should be addressed. E-mail: fuanwang@whu.edu.cn.

# Table of Contents

**Table S1.** The DNA sequences used for the amplified sensing platform.

| No. | Sequence (5'→3') |
|---|---|
| **$L_{1a}$** | 5'-AAG ATA ATG ATC AGA GAT CTC CGA CAC TC-3' |
| **$L_{2a}$** | 5'-GCT TCA TCT TCA TCT CTG ATC ATT ATC TT-3' |
| **$L_{1b}$** | 5'-AAG ATA ATG ATC AGA GAC TCC GAC ACT C-3' |
| **$L_{2b}$** | 5'-GCT TCA TCT TCA TTC TCT GAT CAT TAT CTT-3' |
| **$L_1$** | 5'-AAG ATA ATG ATC AGA GAC CGA CAC TC-3' |
| **$L_2$** | 5'-GCT TCA TCT TCA TCT TCT CTG ATC ATT ATC TT-3' |
| **$L_{1c}$** | 5'-AAG ATA ATG ATC AGA GAA CAC TC-3' |
| **$L_{2c}$** | 5'-GCT TCA TCT TCA TCT CCG TCT CTG ATC ATT ATC TT-3' |
| **$H_{1a}$** | 5'-CTA TCA TTA TCT TGC TTC ATC TTC ATC AAG ATA ATG ATA GAG ACC GAC ACT C-3' |
| **$H_{1b}$** | 5'-CTC TAT CAT TAT CTT GCT TCA TCT TCA TCA AGA TAA TGA TAG AGA CCG ACA CTC-3' |
| **$H_1$** | 5'-GTC TCT ATC ATT ATC TTG CTT CAT CTT CAT CAA GAT AAT GAT AGA GAC CGA CAC TC-3' |
| **$H_2$** | 5'-GCT TCA TCT TCA TCT TCT CTA TCA TTA TCT TGA TGA AGA TGA AGC AAG ATA AT-3' |
| **$H_3$** | 5'-GAG TGT CGG AGA TGA AGA TGA AGC CAT CGT GCT TCA TCT TCA TCT CCG-TAMRA-3' |
| **$H_4$** | 5'-GCT TCA TCT TCA TCT CCG GTT TTG CGG AGA TGA AGA TGA AGC ACG ATG-3' |
| **$H_5$** | 5'-FAM-CAA AAC CGG AGA TGA AGA TGA AGC TTG CCT GCT TCA TCT TCA TCT CCG-3' |
| **$H_6$** | 5'-GCT TCA TCT TCA TCT CCG ACA CTC CGG AGA TGA AGA TGA AGC AGG CAA-3' |
| **$H_{7a}$** | 5'-TCA ACA TCA GTC TGA TAA GCT AGA GTG TCG GTC TCT ATC ATT ATC TTC TAG CTT ATC AGA-3' |
| **$H_{7b}$** | 5'-TCA ACA TCA GTC TGA TAA GCT AGA GTG TCG GTC TCT ATC ATT ATC TTC TAG CTT ATC AGA CT-3' |
| **$H_7$** | 5'- TCA ACA TCA GTC TGA TAA GCT AGA GTG TCG GTC TCT ATC ATT ATC TTC TAG CTT ATC AGA CTG A-3' |
| **$H_{7c}$** | 5'- TCA ACA TCA GTC TGA TAA GCT AGA GTG TCG GTC TCT ATC ATT ATC TTC TAG CTT ATC AGA CTG ATG-3' |
| **I** | 5'-GAG TGT CGG TCT CTA TCA TTA TCT T-3' |
| **$I_a$** | 5'-GAG **A**GT CGG TCT CTA TCA TTA TCT T-3' |
| **$I_b$** | 5'-GAG **A**GT CGG **A**CT CTA TCA TTA TCT T-3' |
| **$I_c$** | 5'-GAG **A**GT CGG **A**CT CTA TC**T** TTA TCT T-3' |
| **T** | 5'-GCT TCA TCT TCA TCT CCG ACA CTC-3' |
| **miR-21** | 5'-UAG CUU AUC AGA CUG AUG UUG A-3' |
| **Let-7a** | 5'-UGA GGU AGU AGG UUG UAU AGU U-3' |
| **Son DNA** | 5'-ACU CCC AGA UGU UAG CAA C-3' |
| **β-actin mRNA** | 5'-GCA AGC CAU GUA CGU UGC UAU CCA GGC UGU GCU AUC CCU GU-3' |

**Table S2.** The DNA sequences used to construct the CHA-HCR imaging system.

| No. | Sequence (5'→3') |
|---|---|
| **$H_1$*** | 5'-G*T*C* TCT ATC ATT ATC TTG CTT CAT CTT CAT CAA GAT AAT GAT AGA GAC CGA CAC* T*C*-3' |
| **$H_2$*** | 5'-G*C*T* TCA TCT TCA TCT TCT CTA TCA TTA TCT TGA TGA AGA TGA AGC AAG ATA* A*T*-3' |
| **$H_3$*** | 5'-G*A*G* TGT CGG AGA TGA AGA TGA AGC CAT CGT GCT TCA TCT TCA TCT *C*C*G-TAMRA-3' |
| **$H_4$*** | 5'-G*C*T* TCA TCT TCA TCT CCG GTT TTG CGG AGA TGA AGA TGA AGC ACG *A*T*G-3' |
| **$H_5$*** | 5'-FAM-C*A*A* AAC CGG AGA TGA AGA TGA AGC TTG CCT GCT TCA TCT TCA TCT *C*C*G-3' |
| **$H_6$*** | 5'-G*C*T* TCA TCT TCA TCT CCG ACA CTC CGG AGA TGA AGA TGA AGC AGG *C*A*A-3' |
| **$H_7$*** | 5'- T*C*A* ACA TCA GTC TGA TAA GCT AGA GTG TCG GTC TCT ATC ATT ATC TTC TAG CTT ATC AGA CT*G* A* -3' |
| **miR-21 inhibitor** | 5’-mU*mC*mA* mAmCmA mUmCmA mGmUmC mUmGmA mUmAmA mG*mC*mU *mA-3’ |

* = Phosphorothioate Bonds

mN = 2’-*O*-Me RNA base

**Table S3. Comparison of different enzyme-free systems for nucleic acid detection**

| System | Reaction time (h) | Sensitivity (M) | Ref. |
|---|---|---|---|
| Catalytic hairpin assembly-mediated mRNA imaging in living cells | 2 | $5\times10^{-10}$ | [1] |
| HCR-mediated in situ visualization of tumor-related mRNA in living cells | 4 | $1.8\times10^{-11}$ | [2] |
| Amplified analysis of DNA through an autocatalytic and catabolic DNAzyme-mediated process | 12 | $1\times10^{-12}$ | [3] |
| Amplified detection of DNA via target-CHA-DNAzyme cascade | 2 | $2\times10^{-11}$ | [4] |
| Multiplexed analysis of genes using nucleic acid-stabilized silver nanoclusters | ~1 | $1\times10^{-9}$ | [5] |
| Fluorescent DNA assay based on DNA-detachment of AgNCs from GO nanohybrids | 1.33 | $1\times10^{-9}$ | [6] |
| Sensitive miRNA assay based on $MnO_2$-mediated signal amplifications in living cells | 4 | $2.5\times10^{-9}$ | [7] |
| CHA-HCR-mediated nucleic acid detection for miRNA imaging | 5 | $2\times10^{-12}$ | This work |

## Schematic illustration of the upstream CHA circuit

A CHA reaction consists of two hairpin DNA structures, **H**$_1$ and **H**$_2$, which are designed to contain the appropriate sequences (where domain x is complementary to domain x*). **H**$_1$ is functionalized at its 3'-end of the stem region with the encoded sequence, d*, that corresponds to one subunit of the two split segments of the HCR trigger sequence. Domain d* is linked to the conserved sequence composed of domains c*-b*-a* and a-b. **H**$_1$ includes the recognition sequence of the target **I**. **H**$_2$ consists of the other subunit c* of the split segments of HCR trigger. This subunit domain c* is linked to the programmed conserved sequences a-b-c and b*, which are complementary to domains c*-b*-a* and b of **H**$_1$, respectively. As shown in **Figure S1**, the initiator **I** triggers the opening of hairpin **H**$_1$ to yield the DNA assembly "**I-H**$_1$" and the release of single-stranded domain b-c* to open hairpin **H**$_2$, yielding an intermediate structure "**I-H**$_1$**·H**$_2$" that stimulates the strand displacement of **I** to regenerate **I** and to yield numerous dsDNA product "**H**$_1$**·H**$_2$". The released initiator strand allows the following activation of the CHA circuit that stimulates successive hybridizations between hairpins **H**$_1$ and **H**$_2$.

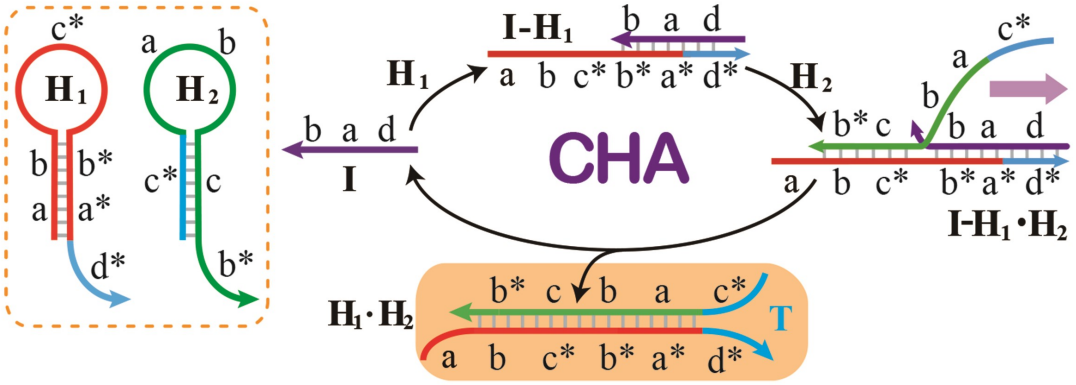


**Figure S1.** The scheme of upstream CHA to generate multiple HCR triggers.

## Schematic illustration of the downstream HCR circuit

Hairpins **H3**, **H4**, **H5** and **H6**, are used for assembling HCR circuit. **H3** is functionalized at its 3'-end with a fluorophore acceptor (TAMRA). **H3** consists of the programmed sequences e-c* and d-c, which are complementary to domains c-e* of **H4** and c*-d* of **H6**. Domain d-c of **H3** acts as the recognition sequence for the generated HCR trigger of co-localized CHA product **T**, "**H1·H2**". **H4** consists of the conserved domains c*-f* and c-e* while **H5** consists of domains f-c and g-c*. **H5** is functionalized at its 5'-end with a fluorophore donor (FAM). **H6** is composed of domains c*-d* and c-g*, which is complementary to domain d-c of **H3** and domain g-c* of **H5**, respectively. As shown in **Figure S2**, the CHA product brings the two subunits of HCR initiator, domains c* and d*, into close proximity, resulting in the structure "**T**" to open **H3** for forming the intermediate structure "**T-H3**". The released domain e-c* of "**T-H3**" hybridizes with domain c-e* of **H4** and opens **H4** to yield structure "**T-H3·H4**". The resulting structure "**T-H3·H4**" hybridizes with domain f-c of **H5**, yielding structure "**T-H3·H4·H5**" that brings two fluorophores FAM and TAMRA into close proximity for generating FRET signal. The released domain g-c* of "**T-H3·H4·H5**" opens **H6** to yield domain c*-d* with the same sequence as **T**-analog structure. The **T**-analog structure furtherly activates the subsequent autonomous sequential and cyclic hybridizations between hairpins **H3**, **H4**, **H5** and **H6**.

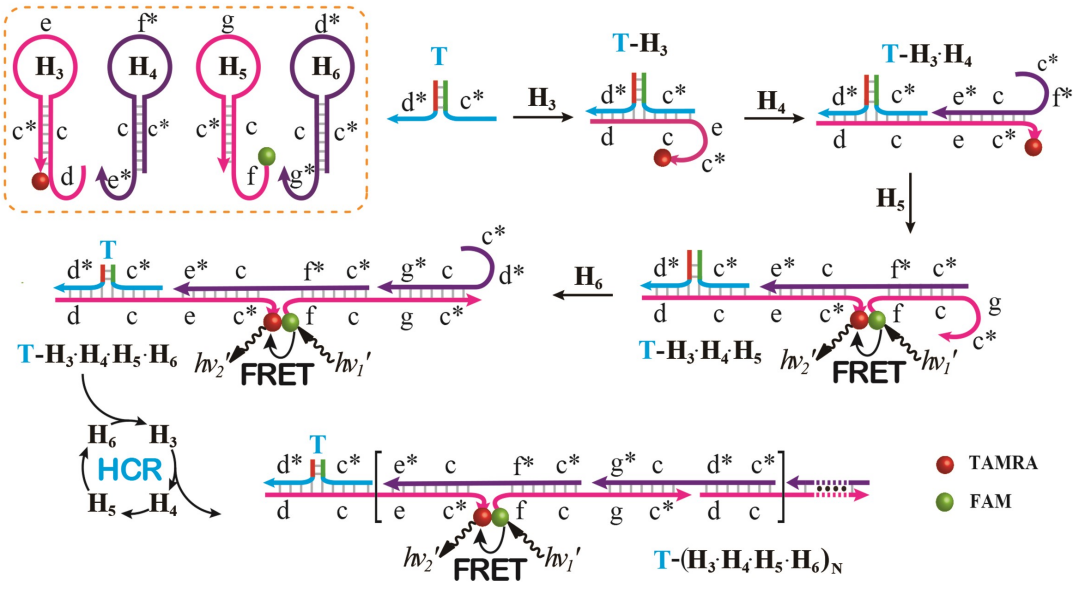


**Figure S2**. The scheme for downstream HCR to transduce the colocalized structure **T** of upstream CHA products into an amplified FRET readout signal.

**Supporting Information**

## Sequence optimization of the CHA-HCR circuit

To achieve a robust DNA sensing platform of higher performance, the substrate hairpins need to be optimized to improve the signal-to-background ratio of CHA-HCR amplifier. We systematically studied the impact of the co-localized toehold and branch-migration domain of CHA product and the stability of the hairpin $\mathbf{H_1}$ on the kinetics of the CHA-HCR circuit. First, different pairs of the subunits of structure "**L**" (domains c* and d*) were incorporated into the substitute ssDNA of hairpin components, such as $\mathbf{L_{1a}}$/$\mathbf{L_{2a}}$, $\mathbf{L_{1b}}$/$\mathbf{L_{2b}}$, $\mathbf{L_1}$/$\mathbf{L_2}$ and $\mathbf{L_{1c}}$/$\mathbf{L_{2c}}$ with the split bases distributions of 12/12, 10/14, 8/16 and 6/18, respectively (**Figure S3**(A)). The kinetically tracing HCR circuits with different structures "**L**" were utilized to evaluate the performance of the amplified DNA assay, **Figures S3**(B) and **S3**(C). $\mathbf{L_1}$/$\mathbf{L_2}$ shows the best performance, which is presumably attributed to the proper toehold-mediated strand displacement of structure "**T**" and $\mathbf{H_3}$. Furthermore, the stem domain of $\mathbf{H_1}$ was optimized to improve the performance of CHA-HCR circuit. Three hairpins, $\mathbf{H_{1a}}$, $\mathbf{H_{1b}}$, $\mathbf{H_1}$, encoded respectively with 14, 16 and 18 bp in the stem domain, were introduced to investigate the system, **Figures S3(**D) and **S3(**E). The absolute fluorescence intensities (-ΔF) of the background decrease obviously with the increasing stem length of $\mathbf{H_1}$ (curves a, c, and e), while that of the initiator-triggered CHA-HCR maintain at a comparably constant level (curves b, d, and f). Accordingly, the hairpin $\mathbf{H_1}$ and the appropriate distribution (similar with $\mathbf{L_1}$/$\mathbf{L_2}$) of HCR trigger was chosen as the optimized substrate for the following experiment.

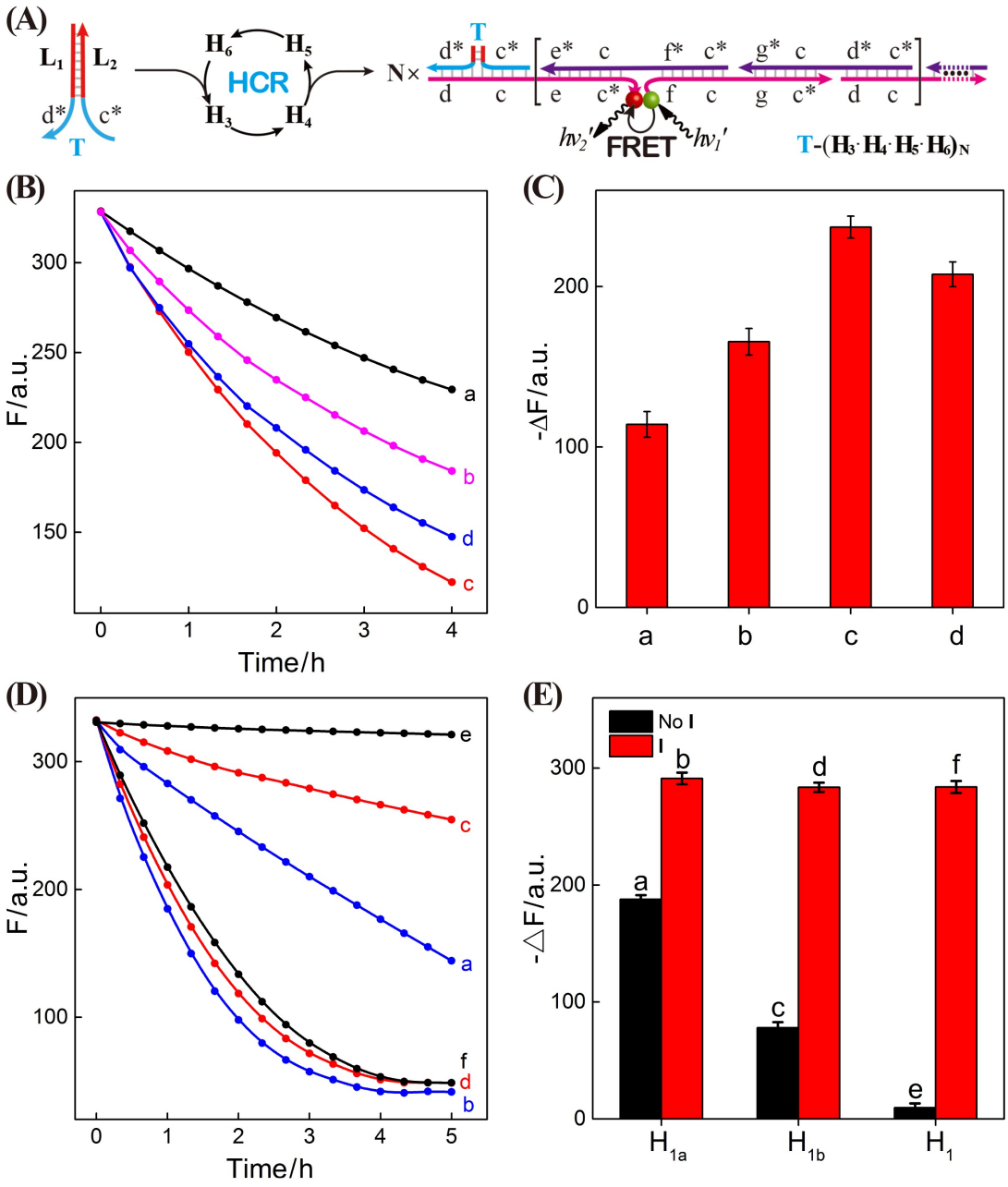


**Figure S3**. (A) Schematic optimization of HCR trigger. Time-dependent fluorescence changes at λ = 520 nm (B) and the absolute fluorescence intensities (-ΔF) for a fixed time interval of 4 h (C) by incubating HCR, composed of **H3** (400 nM), **H4** (200 nM), **H5** (200 nM) and **H6** (200 nM), with 100 nM of the structure "**L**" with different components: **L1a**/**L2a** (a), **L1b**/**L2b** (b), **L1c**/**L2c** (c) and **L1**/**L2** (d). Time-dependent fluorescence changes at λ = 520 nm (D) and the absolute fluorescence intensity (-ΔF) for a fixed time interval of 5 h (E) by incubating **H2** (200 nM), **H3** (400 nM), **H4** (200 nM), **H5** (200 nM) and **H6** (200 nM) with different reactants: 400 nM **H1a** without (a) and with (b) 50 nM initiator, 400 nM **H1b** without (c) and with (d) 50 nM initiator, 400 nM **H1** without (e) and with (f) 50 nM initiator. All reactions were carried out in 10 mM HEPES buffer (pH 7.2) containing 1 M NaCl and 50 mM $MgCl_2$. Error bars were derived from n=5 experiments.

## Temperature optimization of the CHA-HCR circuit

To investigate the influence of temperature on the performance of the CHA-HCR circuit, the this integrated system was carried out under varied temperature conditions (25 °C, 30 °C and 37 °C), **Figure S4**. The fluorescence spectra of the CHA-HCR circuit without (curve a, c and e) or with (curve b, d and f) 50 nM initiator at 5 h were nearly identical under these different temperature conditions, indicating that the temperature has little influence on the proposed CHA-HCR system. It is reasonable since all of our optimization process (including sequence design and buffer designation) is based on an appropriate operation of downstream HCR system that leads to an obvious transduction readout signal. Thus we chose 25 °C as the appropriate temperature for *ex situ* fluorescence experiment and 37 °C for the subsequent *in situ* intracellular imaging experiment.

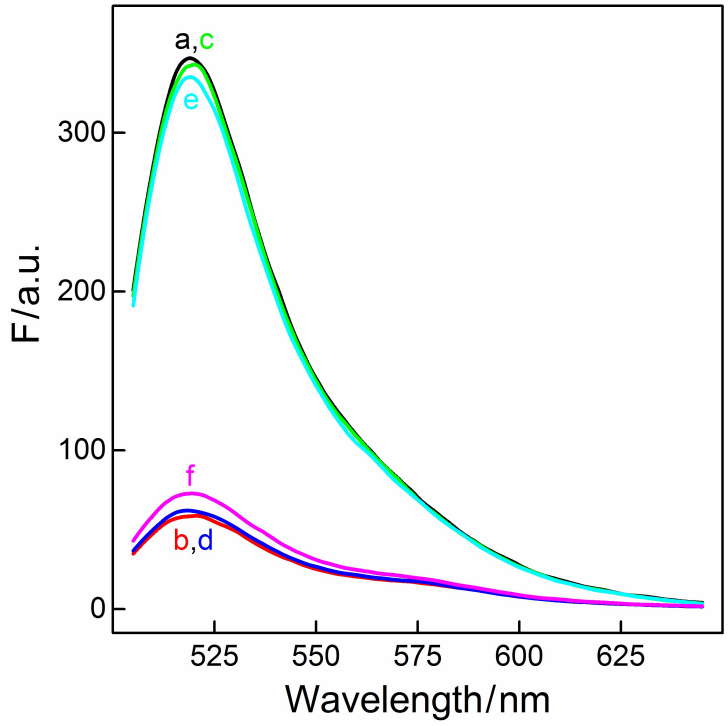


**Figure S4**. Fluorescence spectra of the CHA-HCR circuit upon their incubation with 50 nM initiator **I** for a fixed time interval of 5 h at 25 °C (b), 30 °C (d), and 37 °C (f). Fluorescence spectra of the non-activated CHA-HCR circuit at 25 °C (a), 30 °C (c), and 37 °C (e). All reactions consisting of $\mathbf{H_1}$ (400 nM), $\mathbf{H_2}$ (400 nM), $\mathbf{H_3}$ (400 nM), $\mathbf{H_4}$ (200 nM), $\mathbf{H_5}$ (200 nM) and $\mathbf{H_6}$ (200 nM) were carried out in 10 mM HEPES buffer (pH 7.2, 1 M NaCl, 50 mM $MgCl_2$).

## Comparison of CHA and HCR systems with the CHA-HCR circuit

A traditional HCR system was obtained by incubating **T** with HCR reactant hairpins **H**$_3$, **H**$_4$, **H**$_5$ and **H**$_6$ while the upstream CHA was expelled from the integrated system. Then only the downstream HCR was activated to generate FRET readout signal. Also the **H**$_6$-excluded CHA-HCR system was adapted as a conventional CHA system where the intact CHA carried out single-stage amplification and the subsequent **H**$_6$-expelled HCR executed merely as a signal readout device. As shown in **Figure S5**, the CHA-HCR system showed a much higher fluorescence change (curve d) over that of traditional HCR (curve c) or CHA (curve b), demonstrating the enhanced signal amplification efficiency of the CHA-HCR circuit than conventional HCR or CHA circuit.

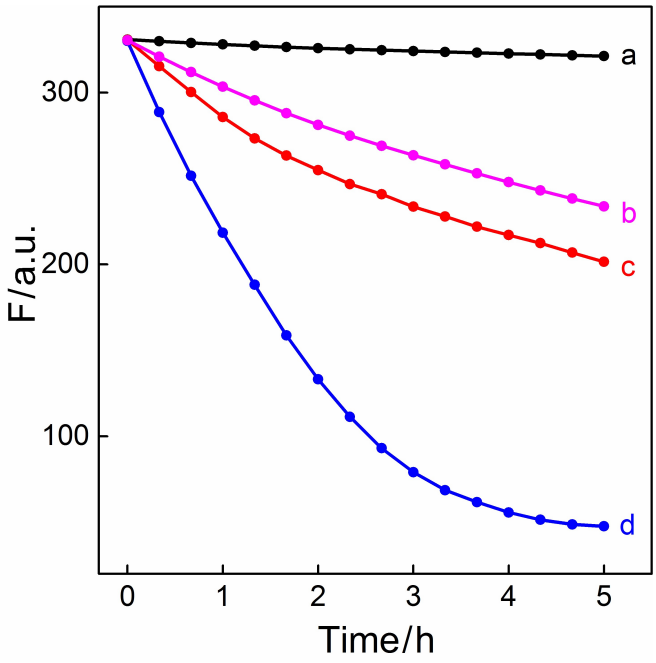


**Figure S5**. Time-dependent fluorescence changes (at λ = 520 nm) of the CHA-HCR circuit, composed of **H**$_1$ (400 nM), **H**$_2$ (400 nM), **H**$_3$ (400 nM), **H**$_4$ (200 nM), **H**$_5$ (200 nM) and **H**$_6$ (200 nM), without (a) and with (d) 50 nM initiator **I**, the traditional CHA circuit (b) by incubation **H**$_1$ (400 nM), **H**$_2$ (400 nM), **H**$_3$ (400 nM), **H**$_4$ (200 nM) and **H**$_5$ (200 nM) with 50 nM initiator **I**, and the conventional HCR circuit (c) by incubation **H**$_3$ (400 nM), **H**$_4$ (200 nM), **H**$_5$ (200 nM) and **H**$_6$ (200 nM) with initiator **T** (50 nM). All reactions were carried out in 10 mM HEPES buffer (pH 7.2) containing 1 M NaCl and 50 mM $MgCl_2$.

## Demonstration of the indispensable role of CHA-HCR components

By subtracting **H**$_1$ or **H**$_2$ from upstream CHA, or by subtracting **H**$_4$ from downstream HCR, no fluorescence change can be observed, **Figure S7**(A), **S7**(B) and **S7**(C), respectively. However, a moderate fluorescence change was emerged for **I**-initiated **H**$_6$-expelled CHA-HCR system, **Figure S7**(D). It can be explained that only the upstream CHA acts as single-stage amplifier by successively producing multiple colocalized HCR trigger sequence for **H**$_6$-excluded downstream HCR, which merely acts as a stoichiometric transduction device. It is clear that the amplification capability of CHA system is lower than that of concatenated CHA-HCR circuit, and each component of these CHA-HCR mixture is indispensable for executing the synergistic amplification procedure.

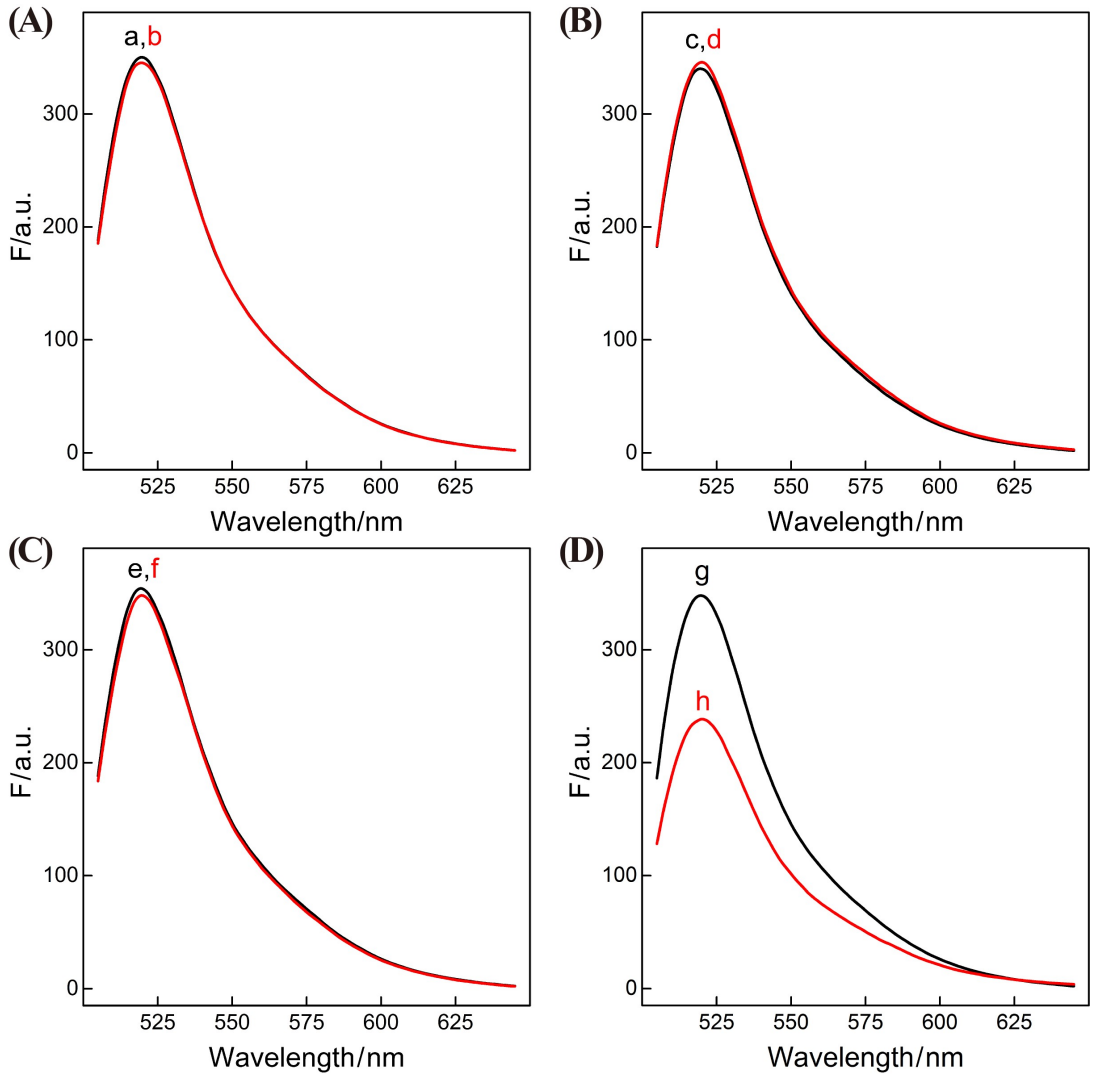


**Figure S6**. (A) Fluorescence spectra generated by the mixture of **H**$_2$ (400 nM), **H**$_3$ (400 nM), **H**$_4$ (200 nM), **H**$_5$ (200 nM) and **H**$_6$ (200 nM) in the presence of no initiator (a) and 50 nM initiator (b). (B) Fluorescence spectra generated by the mixture of **H**$_1$ (400 nM), **H**$_3$ (400 nM), **H**$_4$ (200 nM), **H**$_5$ (200 nM) and **H**$_6$ (200 nM) in the presence of no initiator (c) and 50 nM initiator (d). (C) Fluorescence spectra generated by the mixture of **H**$_1$ (400 nM), **H**$_2$ (400 nM), **H**$_3$ (400 nM), **H**$_5$ (200 nM) and **H**$_6$ (200 nM) in the presence of no initiator (e) and 50 nM initiator (f). (D) Fluorescence spectra generated by the mixture of **H**$_1$ (400 nM), **H**$_2$ (400 nM), **H**$_3$ (400 nM), **H**$_4$ (200 nM) and **H**$_5$ (200 nM) in the presence of no initiator (g) and 50 nM initiator (h). All reactions were carried out for a fixed time interval of 5 h in 10 mM HEPES buffer (pH 7.2) containing 1 M NaCl and 50 mM $MgCl_2$.

## Performance of conventional CHA and HCR systems

The kinetic analysis of the merely CHA and HCR systems were carried out to show indirectly the clear pathway of CHA-HCR circuit (**Figures S7(A)** and **7(B)**, respectively). Here the **H**$_6$-excluded CHA-HCR system was adapted as a conventional CHA system where the intact CHA carried out single-stage amplification and the subsequent **H**$_6$-expelled HCR executed merely as a signal readout device (**Figure S7(A)**). The fluorescence readout did not reach its saturation value at the fixed time-interval of 5 h even with a high concentration of analyte **I** (50 nM). With an increasing concentration of analyte from 5 to 50 nM, the absolute fluorescence changes (-ΔF) of CHA reaction increased slowly, while nearly no fluorescence change was observed for the CHA mixture that was incubated with lower concentration of analyte **I** (less than 5 nM). Similarly, the kinetically monitoring conventional HCR process was proceeded (**Figures S7(B)**). The fluorescence reaches an unsaturated value even with a high concentration of analyte (50 nM) when the reaction time exceeds 5 h. A dramatically lower fluorescence response was observed for single CHA or HCR circuit as compared with the cascaded CHA-HCR system at a fixed time-interval of 5 h, validating the significant signal amplification of our CHA-HCR circuit. By integrating the first-stage signal amplification of CHA and the second-stage amplification of HCR, the high performance of our CHA-HCR amplifier is attributed to its inherent synergistically accelerated recognitions and hybridizations of these CHA or HCR constitutes.

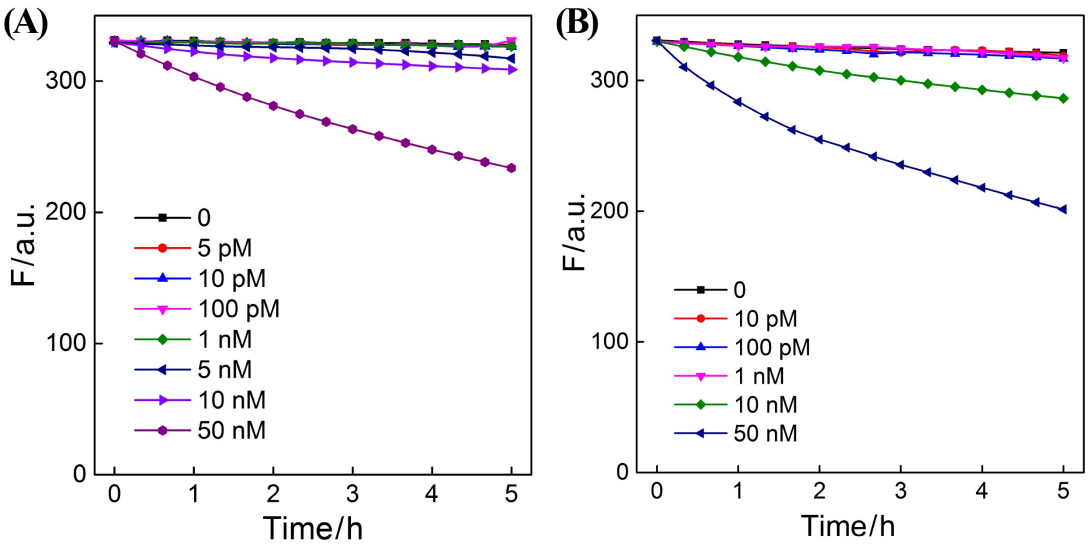


**Figure S7** (A) Time-dependent fluorescence changes (at λ = 520 nm) of traditional CHA circuit, composed of **H**$_1$ (400 nM), **H**$_2$ (400 nM), **H**$_3$ (400 nM), **H**$_4$ (200 nM) and **H**$_5$ (200 nM) with different concentrations of initiator **I**. (B) Time-dependent fluorescence changes (at λ = 520 nm) of conventional HCR circuit, composed of **H**$_3$ (400 nM), **H**$_4$ (200 nM), **H**$_5$ (200 nM) and **H**$_6$ (200 nM) with different concentrations of **T**. All reactions were carried out in 10 mM HEPES buffer (pH 7.2) containing 1 M NaCl and 50 mM $MgCl_2$.

**Supporting Information**

**The specificity of the CHA-HCR system**

To investigate the specificity of CHA-HCR circuit for amplified DNA detection, the sequences of the one-, two-, and three-base mutants ($\mathbf{I_a}$, $\mathbf{I_b}$ and $\mathbf{I_c}$) were respectively investigated by the concatenated CHA-HCR system. As shown in **Figure S8**, scarcely no fluorescence change was revealed for $\mathbf{I_c}$ (curve d) and it was almost the same with the background response (curve e). Although one-base mutant $\mathbf{I_a}$ (curve b) and two-base mutant $\mathbf{I_b}$ (curve c) induced observable fluorescence changes, these responses could be obviously distinguished from the fully complementary initiator-triggered system. These results demonstrated the high specificity of the CHA-HCR sensing platform.

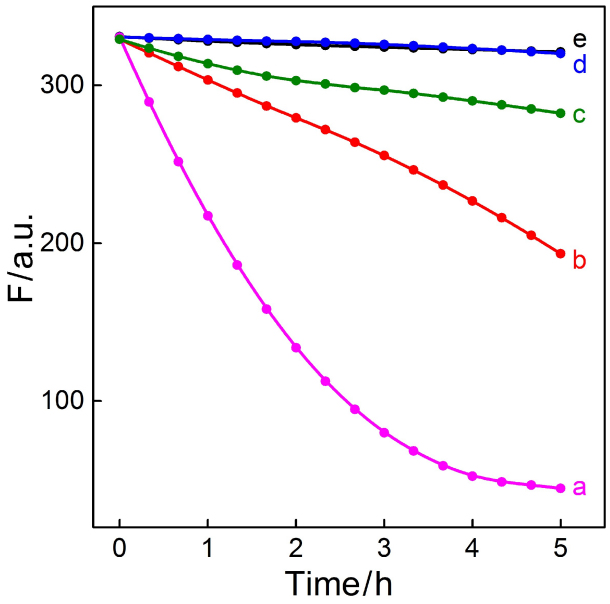


**Figure S8**. Time-dependent fluorescence changes (at λ = 520 nm) of the CHA-HCR system upon analysis of different analytes: (a) 50 nM **I**, (b) 50 nM $\mathbf{I_a}$, (c) 50 nM $\mathbf{I_b}$, (d) 50 nM $\mathbf{I_c}$, and (e) no analyte. The system consisting of $\mathbf{H_1}$ (400 nM), $\mathbf{H_2}$ (400 nM), $\mathbf{H_3}$ (400 nM), $\mathbf{H_4}$ (200 nM), $\mathbf{H_5}$ (200 nM) and $\mathbf{H_6}$ (200 nM) was carried out in 10 mM HEPES buffer (pH 7.2) containing 1 M NaCl and 50 mM $MgCl_2$.

## Optimization of sensing module for analyzing miR-21

The generalized miR-21 sensing platform is constructed by integrating the CHA-HCR circuit with a "helper" hairpin acting as functional recognition device. The stem region of "helper" hairpin was designed to include a partially complementary sequence of miR-21, and the loop of **H**$_7$ was inserted with the initiator sequence of CHA-HCR circuit. As indicated in **Figure S9**(A), once the helper hairpin recognized and hybridized with miR-21, the opened hairpin released the initiator for triggering CHA-HCR circuit and generating FRET signal. Since the CHA-HCR-composed amplification module has been already optimized, then the performance of miR-21-targeting sensing system are closely related with the auxiliary helper hairpin that needs to be investigated to get a higher signal-to-back ground ratio ($\triangle F_S/\triangle F_B$). Four different miR-21-targeting hairpins (**H**$_{7a}$, **H**$_{7b}$, **H**$_7$ and **H**$_{7c}$) were designed to contain different length (13, 15, 18 and 20, respectively) of stem regions and integrated into the CHA-HCR circuit for detecting miR-21 analyte, **Figure S9**(B). The background of the system decreased with the increasing stem length and reached a saturated value with stem length of 18 and 20, suggesting that the stability of helper hairpin plays a key role in this process. The fluorescence changes of the triggered CHA-HCR mixture are nearly the same when the length of stem region corresponds to 13, 15 and 18 and then it decreased sharply with the stem region reaches to 20. It means the hairpin is too stable to be opened by the miR-21 target and to trigger the CHA-HCR amplifier. Thus the 18-bp auxiliary hairpin **H**$_7$ was chosen as the optimized helper hairpin and was then introduced into the present CHA-HCR amplifier for detecting miR-21.

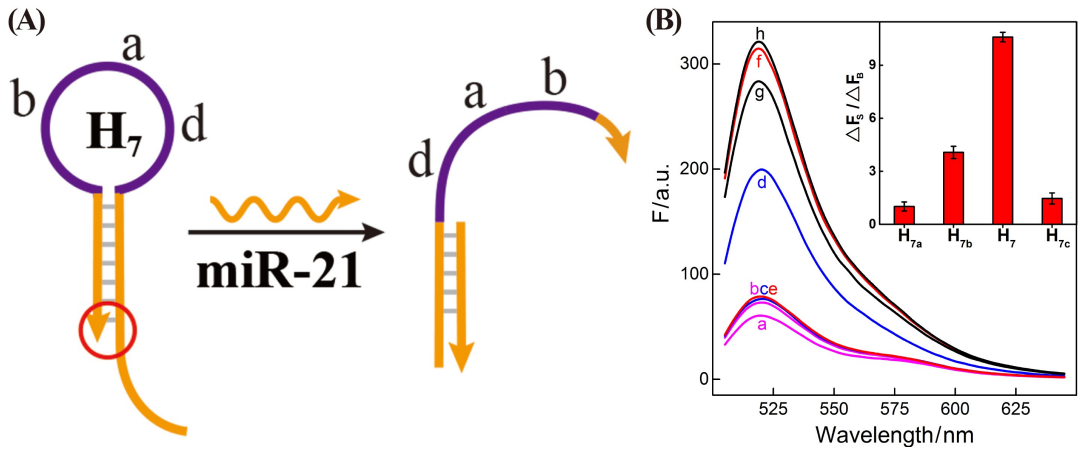


**Figure S9.** (A) Schematically opening of the "helper" hairpin **H**$_7$ for the generalized and amplified detection of miR-21. (B) Fluorescence spectra of the miR-21 sensing system for a fixed time interval of 5 h by incubating **H**$_1$ (400 nM), **H**$_2$ (400 nM), **H**$_3$ (400 nM), **H**$_4$ (200 nM), **H**$_5$ (200 nM) and **H**$_6$ (200 nM) with different "helper" hairpin: 50 nM **H**$_{7a}$ with (curve a) and without (curve b) 5 nM miR-21, 50 nM **H**$_{7b}$ with (curve c) and without (curve d) 5 nM miR-21, 50 nM **H**$_7$ with (curve e) and without (curve f) 5 nM miR-21, and 50 nM **H**$_{7c}$ with (curve g) and without (curve h) 5 nM miR-21. Inset: $\triangle F_S/\triangle F_B$ ratio represents the signal-to-background ratio of the respective system. The reaction was carried out in 10 mM HEPES buffer (pH 7.2) containing 1 M NaCl and 50 mM $MgCl_2$. Error bars were derived from n=5 experiments.

## The selectivity of the miR-21 sensing platform

To evaluate the selectivity of the present CHA-HCR system for miR-21 detection, three control nucleic acids, β-actin mRNA, let-7a miRNA and son DNA were assessed with the present sensing system. As illustrated in **Figure S10**, the fluorescence spectra was almost the same as the background signal (curves a) upon analyzing these control analytes (curves b, c and d), while a significantly decreased fluorescence spectra was observed for miR-21-initiated CHA-HCR circuit (curve e). It clearly demonstrates a high selectivity of the present miR-21-sensing platform that is likely to discriminate target miRNA from its interfering sequences in complex biological environment.

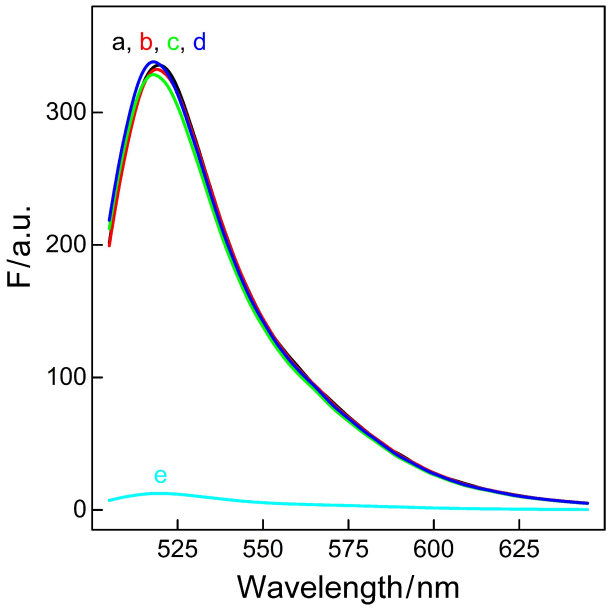


**Figure S10.** Fluorescence spectra of the miR-21-targeting system upon analyzing different analytes for a fixed time-interval of 5 h: (a) no analyte, (b) 50 nM β-actin mRNA, (c) 50 nM let-7a, (d) 50 nM son DNA and (e) 50 nM miR-21. The system consisting of $\mathbf{H_1}$ (400 nM), $\mathbf{H_2}$ (400 nM), $\mathbf{H_3}$ (400 nM), $\mathbf{H_4}$ (200 nM), $\mathbf{H_5}$ (200 nM), $\mathbf{H_6}$ (200 nM) and $\mathbf{H_7}$ (50 nM) was carried out in 10 mM HEPES buffer (pH 7.2) containing 1 M NaCl and 50 mM $MgCl_2$.

## CHA-HCR imaging of miR-21 in living cells

Besides the high sensitivity and selectivity of the CHA-HCR imaging system, accurate signal transduction is also demanded to avoid undesirable interfere from surrounding complex cellular environment. Here the fluorescence ratio of FRET to FAM ($F_{FRET}/F_{FAM}$) was adapted as the FRET imaging signal to investigate the different expression levels of miR-21 in different cell lines. As shown in **Figure S11**, the CLSM investigations (including FAM, FRET and the bright field-included FRET merge images) of different cells were carried out after transfecting and incubating the corresponding samples at 37 °C for 5 h. An obvious FRET signal ($F_{FRET}/F_{FAM}$) was observed for CHA-HCR-mediated imaging MCF-7 cells (sample a), implying that miR-21 was overexpressed in MCF-7 cells as reported. The **$H_6$***-excluded CHA-HCR circuit was also applied to sensing miR-21 in MCF-7 cells and a relatively low FRET signal ($F_{FRET}/F_{FAM}$) was observed for conventional CHA circuit (sample b). To identify the robust FRET readout of varied miR-21 expressions by CHA-HCR amplifier, an inhibitor was used for knocking down miR-21 expressions in MCF-7 cells (sample c). No FRET signal ($F_{FRET}/F_{FAM}$) emerged, indicating the CHA-HCR can discriminate different miR-21 expressions in living cells. Then the miR-21-targeting imaging platform was applied to Hela cells (sample d) with a comparably low FRET signal. It showed great potential for monitoring varied microRNA expressions of different cells.

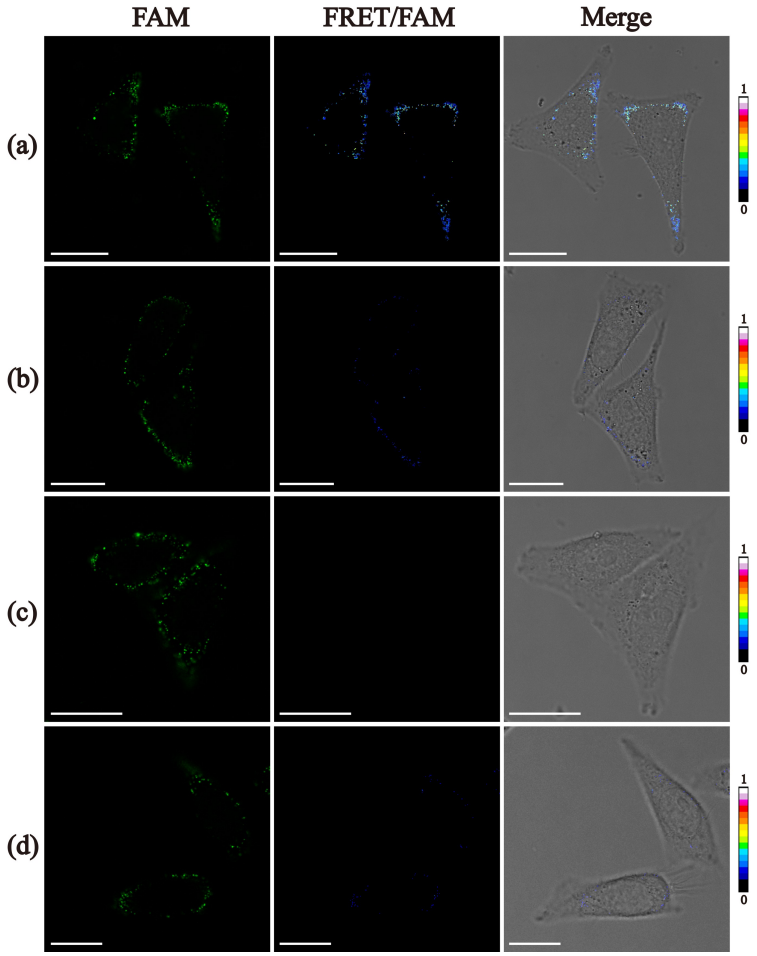


**Figure S11**. Amplified miR-21 imaging in living cells based on CHA-HCR circuit. Confocal laser scanning microscopy imaging of miR-21 in (a) MCF-7 cells by CHA-HCR system, (b) MCF-7 cells by conventional CHA system (**$H_6$***-excluded CHA-HCR), (c) inhibitor-treated MCF-7 cells by CHA-HCR system, and (d) Hela cells by CHA-HCR system. All of the living cells were transfected with miR-21-targeting CHA-HCR system, containing **$H_7$*** (0.05 nmol) and **$H_1$*+$H_2$*+$H_3$*+$H_4$*+$H_5$*+$H_6$*** (0.2 nmol each) or conventional CHA system, containing **$H_7$*** (0.05 nmol) and **$H_1$*+$H_2$*+$H_3$*+$H_4$*+$H_5$*** (0.2 nmol each) at 37 °C for a fixed time-interval of 5 h. Scale bars correspond to 20 μm.

## Optimization of incubation time for CHA-HCR imaging platform

As a prerequisite intracellular imaging experiment, the time-dependent imaging experiment has been executed to get the most appropriate incubation time. We transfected the CHA-HCR mixture into MCF-7 cells by lipofectamine 3000 for different time-intervals. Then these cells were washed three times with PBS for CLSM observations. As shown in **Figure S12**, a weak FRET readout ($F_{FRET}/F_{FAM}$) was observed by incubating the imaging system with cells for 1 h, due to an inadequate uptake of the sensing probes and an insufficient reaction of the CHA-HCR amplifier. As the increasing incubation time of CHA-HCR mixture with cells, the FRET readout was gradually increased and reached a saturation value at 5 h, which was consistent with that of the *in vitro* fluorescence experiment. The FRET readout ($F_{FRET}/F_{FAM}$) remained stable from 5 to 6 h, indicating that the CHA-HCR system reached equilibrium with the response to intracellular miR-21 in MCF-7 cells. Considering the intracellular biostability and sensitivity of our CHA-HCR system, 5 h was thus selected as the best incubation time of the autonomous CHA-HCR amplifier for intracellular imaging application.

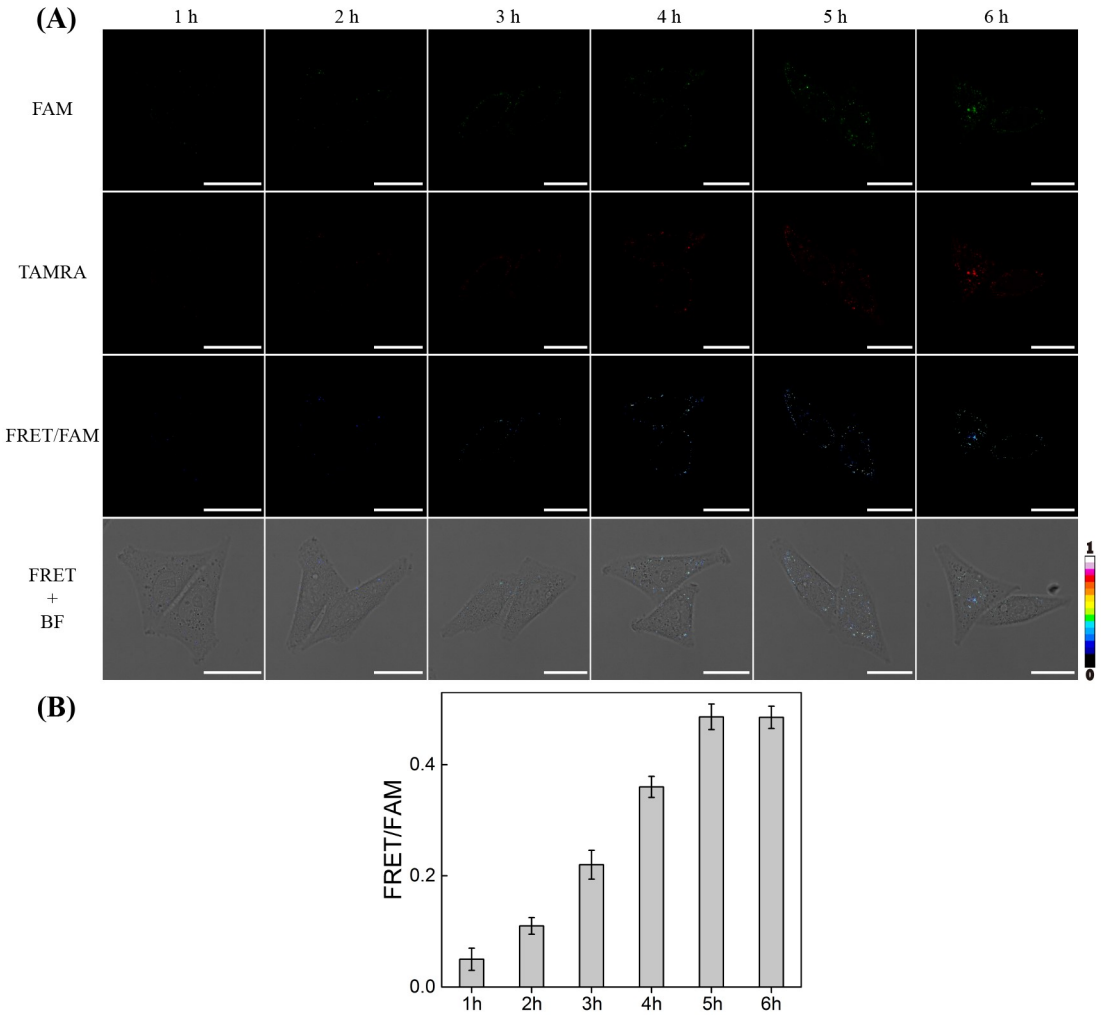


**Figure S12.** Optimization of incubation time for the miR-21-targeting CHA-HCR mixture in MCF-7 living cells. (A) CLSM characterization and (B) the corresponding statistical histogram analysis of FRET readout ($F_{FRET}/F_{FAM}$) by incubating the CHA-HCR mixture with MCF-7 cells for different time-intervals at 37 °C. All scale bars correspond to 20 μm.

## The Z-stacks FRET analysis of miR-21 in MCF-7 live cells

A series of Z-section CLSM images with z step of 0.2 μm throughout the entire cells were captured to integrate the Z-stack projections with a purpose to show the overall FRET readout ($F_{FRET}/F_{FAM}$) of the CHA-HCR imaging system. As shown in the Z-stack projections of MCF-7 cells, it is clear that the miR-21 are localized throughout the entire cells as revealed by their corresponding intracellular FRET signal (**Figure S13**).

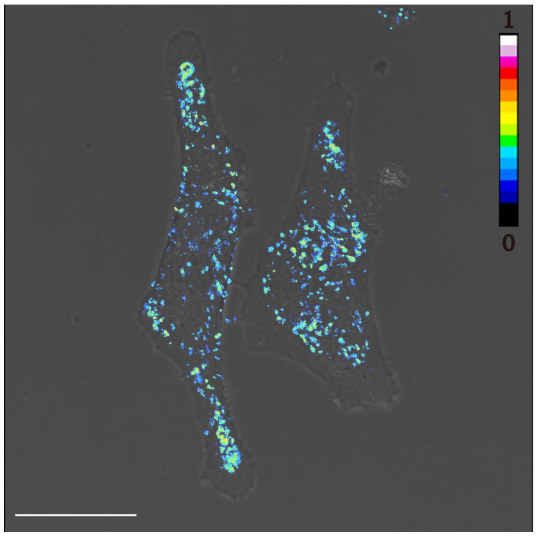


**Figure S13**. FRET analysis of MCF-7 cells by Z-stacks projections consisting of 51 slices stacks at 0.2 μm increments of the entire MCF-7 living cells upon their incubating with CHA-HCR mixture for 5 h at 37 °C. Here the FRET readout was denoted as the fluorescence ratio of FRET to FAM ($F_{FRET}/F_{FAM}$). Scale bars correspond to 20 μm.

## Control experiments for CHA-HCR-mediated miR-21-imaging

To demonstrate the high amplification efficiency of the CHA-HCR system for miR-21 imaging, intracellular control experiments were carried out by removing one of the hairpin components from the CHA-HCR mixture. As shown in **Figure S13**, an obvious FRET imaging signal ($F_{FRET}/F_{FAM}$) was acquired for CHA-HCR system (sample a) while a reduced FRET signal ($F_{FRET}/F_{FAM}$) was observed for conventional CHA imaging system (**H**$_6$*-excluded CHA-HCR mixture, sample b). Moreover, no FRET readout ($F_{FRET}/F_{FAM}$) was observed for **H**$_1$-, **H**$_2$*- or **H**$_4$*-excluded CHA-HCR system (sample c, d or e, respectively), indicating that all of the hairpin reactants were indispensable for the present CHA-HCR circuit. The high amplification efficiency of the two-layered CHA-HCR system is attributed to the synergistically multiple-staged acceleration reactions.

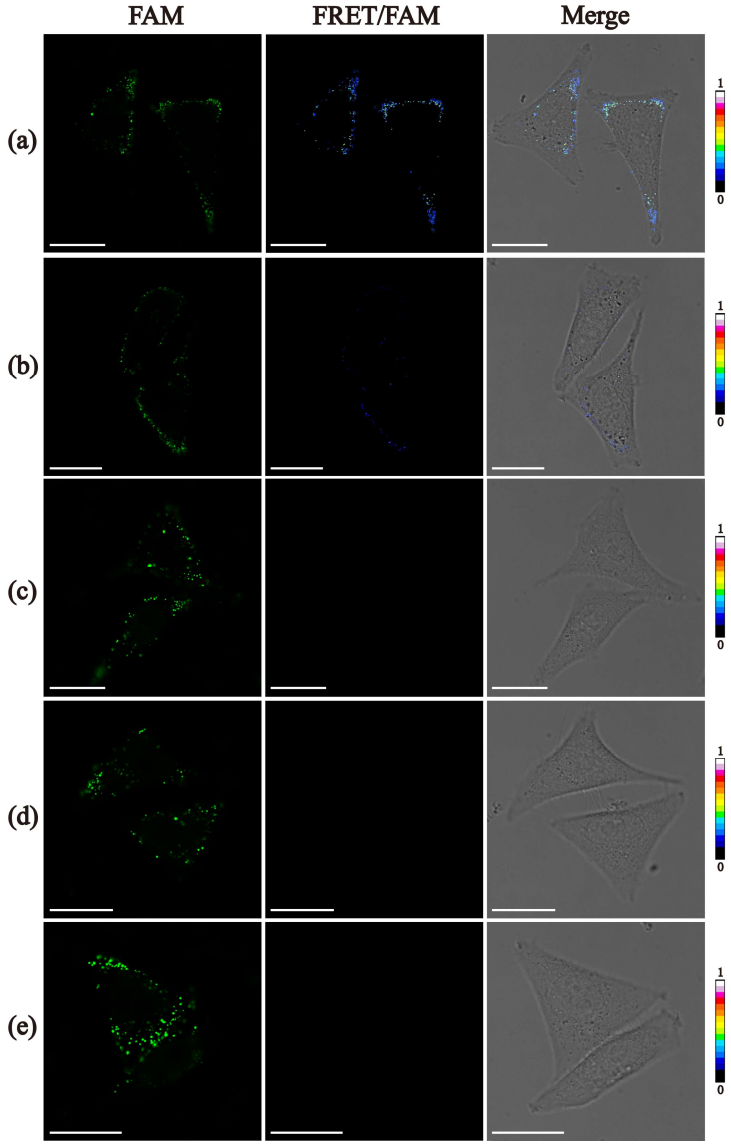


**Figure S14.** Confocal laser scanning microscopy imaging of miR-21 in MCF-7 live cells that were transfected with (a) the intact CHA-HCR system, (b) **H**$_6$*-excluded CHA-HCR system, (c) **H**$_1$*-excluded CHA-HCR system, (d) **H**$_2$*-excluded CHA-HCR system and (e) **H**$_4$*-excluded CHA-HCR system at 37 °C for 5 h. The corresponding dosages of substrates were the same as **Figure S11**. Here the FRET readout was denoted as the fluorescence ratio of FRET to FAM ($F_{FRET}/F_{FAM}$). Scale bars correspond to 20 μm.

## References

[1] C. C. Wu, S. Cansiz, L. Q. Zhang, I. T. Teng, L. P. Qiu, J. Li, Y. Liu, C. Zhou, R. Hu, T. Zhang, C. Cui, L. Cui and W. H. Tan, *J. Am. Chem. Soc.*, 2015, **137**, 4900-4903.

[2] J. Huang, H. Wang, X. Yang, K. Quan, Y. Yang, L. Ying, N. Xie, M. Ou and K. Wang, *Chem. Sci.*, 2016, **7**, 3829-3835.

[3] F. Wang, J. Elbaz, C. Teller and I. Willner, *Angew. Chem., Int. Ed.*, 2011, **50**, 295-299.

[4] A. X. Zheng, J. Li, J. R. Wang, X. R. Song, G. N. Chen and H. H. Yang, *Chem. Commun.*, 2012, **48**, 3112.

[5] N. Enkin, F. Wang, E. Sharon, H. B. Albada and I. Willner, *ACS Nano*, 2014, **8**, 11666-11673.

[6] X. Liu, F. Wang, R. Aizen, O. Yehezkeli and I. Willner, *J. Am. Chem. Soc.*, 2013, **135**, 11832-11839.

[7] J. Li, D. Li, R. Yuan and Y. Xiang, *ACS Appl. Mater. Interfaces*, 2017, **9**, 5717-5724.